Solid-state ion exchange of Fe in small pore SSZ-13 zeolite: Characterization of the exchanged species and their relevance for the NOx SCR reaction

Applied Catalysis A, General 658 (2023) 119160

Contents lists available at ScienceDirect

Applied Catalysis A, General

journal homepage: www.elsevier.com/locate/apcata

Solid-state ion exchange of Fe in small pore SSZ-13 zeolite: Characterization of the exchanged species and their relevance for the NO_x SCR reaction

Ferenc Martinovic, Sabrina Ballauri, Nicola Blangetti, Samir Bensaid, Raffaele Pirone, Barbara Bonelli, Marco Armandi, Fabio Alessandro Deorsola *

Department of Applied Science and Technology, Politecnico di Torino, Corso Duca degli Abruzzi, 24, 10129 Torino, Italy

ARTICLE INFO

Keywords:
Fe ion exchange
Zeolite
Solid state
NOx
Selective catalytic reduction

ABSTRACT

Solid state ion exchange was performed for the successful introduction of Fe cations in the small pore CHA structured SSZ-13 zeolite. The produced catalysts were characterized by IR and UV-Vis spectroscopies and thermally programmed reaction techniques to probe the Fe sites formed during the exchange and the catalytic activity for the NO_x SCR reaction. The results indicate that highly dispersed and heterogeneous Fe sites are formed, and the type depends on the Al distribution in the zeolite. Dimeric Fe species are formed preferentially at the start of the exchange on the 6- and 8-member rings that contain at least two Al exchange sites and once these sites are fully saturated the Fe is exchanged as isolated cations.

1. Introduction

Zeolites with exchanged Cu or Fe have become the primary catalysts for the NH_3 mediated abatement of NO_x, especially in the automotive sector. They are characterized by a wide operating temperature range and high adsorption capacity, that dampen the inherent high variability of temperature and pollutant concentration in the exhaust gas [1–4]. Recently, the Cu-exchanged small cage chabazite type zeotypes (e.g., SSZ-13 zeolite or SAPO-34 silicoaluminophosphate) became dominant in practical applications, largely substituting the medium and large pore diameter zeolites (e.g. MOR, ZSM-5 or BEA). Zeolites with small cage and pore diameter offer better catalytic activity, lower N_2O production during the SCR reaction, higher resistance to hydrocarbon poisoning due to size exclusion effect and better hydrothermal stability. The CHA zeolites are resistant to sintering up to 800 °C, in contrast to 650 °C for larger pore zeolite, and this can be especially relevant in the context of SCR-on-Filter applications that require high temperature regeneration of the filter [5–9]. The Cu-exchanged zeolites are widely investigated and used in practical applications for low temperature (< 350 °C) SCR reaction; however, at higher temperature (> 350 °C) Fe-exchanged zeolites are preferable due to higher NO_x conversion, less N_2O production and more efficient NH_3 utilization [1–9].

The ion exchange of metals in zeolites produces highly dispersed extra-framework metal ions, in some cases even atomic dispersion, and as a result high active site utilization in the desired reaction. The most common ion exchange synthesis method is *liquid ion exchange*, whereby the powdered zeolite is dispersed in a solution containing solvated metal ions. With this method the extent of exchange and metal loading is difficult to control precisely due to a number of factors involved, e.g., temperature, pH, time, counter-ions present in the solution, exchange affinity and pore size effect. Liquid ion exchange also results in large volumes of wastewater that can be challenging to dispose of on industrial scale.

The *solid-state ion exchange* (SSIE) in zeolites has been widely demonstrated for different metals and the reaction is generally thought to occur through ion displacement mechanism [10–16]. The initial widespread research of SSIE was relative to the exchange of La in Y-zeolite for fluid catalytic cracking (FCC). It was observed that La^{3+} ions in aqueous solution have a large hydration diameter and cannot enter the zeolite pore during the liquid ion exchange, while the SSIE method could produce ion exchanged La-Y and La-BEA zeolites [17,18]. For the same reason, the liquid ion exchange of Fe ions in zeolites is difficult, the large diameter of the $Fe[H_2O]_6^{3+}$ complex prevents the entry of ions in the zeolite pores. For the successful liquid ion exchange of Fe in medium and small pore diameter zeolites it is necessary to use Fe^{2+} precursor and ensure the absence of dissolved oxygen in the liquid

* Corresponding author.
E-mail address: fabio.deorsola@polito.it (F.A. Deorsola).

https://doi.org/10.1016/j.apcata.2023.119160
Received 19 January 2023; Received in revised form 21 March 2023; Accepted 22 March 2023
Available online 29 March 2023

through degassing and flowing N_2 [19–21]. Some synthesis methods propose the addition of ascorbic acid as oxygen scavenger and prevent Fe^{2+} to Fe^{3+} conversion [22–24]. Even with these precautions, it is problematic to produce a Fe-zeolite with precisely controlled metal loading.

SSIE of Fe in large and medium pore diameter zeolites (primarily ZSM-5) has been demonstrated as highly efficient synthesis method, reaching high exchange ratio and precisely controlled metal content [13,25–27]. The liquid ion exchange of Fe in CHA framework small pore zeolite is challenging, while the potential of the SSIE method has not yet been reported. The research regarding the coordination, reactivity, and location of Fe species in the small pore zeolites has revealed large variations and multiple Fe types and their roles in catalytic reactions are still actively debated. In this manuscript the process and some of the conditions required for successful Fe SSIE procedure in the SSZ-13 zeolite are explored and discussed. The SSIE process was examined in depth, the physicochemical properties of the obtained Fe zeolites, along with the location/coordination of the Fe sites and the reactivity in the context of NO_x abatement, were studied in detail.

2. Experimental

2.1. Materials

The parent SSZ-13 zeolite was provided by ACS Material (SiO_2/Al_2O_3 = 18, NH_4-form). For the SSIE synthesis, the precursor $FeCl_2{\cdot}4\ H_2O$ was used and it was applied in amounts required to obtain Fe/Al molar ratios of 0.045, 0.067, 0.125 and 0.25. These Fe/Al ratios are included in brackets for the nomenclature used for the labeling of the investigated catalysts, while the Fe content by weight is reported in Table 1. The zeolite and the $FeCl_2{\cdot}4\ H_2O$ powders were placed in a ceramic zirconia grinding jar with zirconia beads and ball-milled in a planetary mill for 0.5 h to obtain tight contact. Following the milling, the powder was placed in the reactor system (see the description below) and inert atmosphere was obtained by flowing He for 1 h. Under He flow the temperature was increased at 2 °C/min rate up to 550 °C and held at that temperature for 0.5 h. Finally, the as-obtained SSIE powder was calcined in air at 650 °C in a muffle furnace. Other samples were synthesized by varying the synthesis conditions as follows:

- Following ball-milling, the catalyst was not heated under inert condition, but immediately calcined in air.
- A sample was prepared through incipient wetness impregnation of the H-SSZ-13 zeolite with $Fe(NO_3)_3{\cdot}6H_2O$.
- SSIE was performed with the H-form of the zeolite (H-SSIE(0.25)) instead of the NH_4 form as for the other samples.

The Fe loading and other physico-chemical characterization results are summarized in Table 1.

A reference sample of Fe-BEA was synthesized using the classical liquid ion exchange method. Deionized water was degassed by flowing N_2 within isolated bubbler after which ascorbic acid was added in concentration of 100 mM, followed by the addition of the H-BEA powder. Fe(II) acetate was added in amount that corresponds to 50 mM of Fe^{2+} solution and the solution was stirred for 24 h after which it was separated by centrifugation and washed. Following the washing step, the sample was dried at 120 °C and calcined in air at 550 °C. Higher calcination temperature resulted in severely deteriorated catalytic activity.

Table 1
Summary of some physico-chemical properties.

Sample	H_2/Fe uptake (mol/mol)	Pore volume (cm^3/g)	Fe content (wt %)
SSIE FeAl = 0.25	0.28	0.21	2.5
SSIE FeAl = 0.125	0.34	0.20	1.25
SSIE FeAl = 0.067	0.38	0.22	0.67
SSIE FeAl = 0.045	0.5	0.21	0.44
H-SSZ-13	-	0.25	-

2.2. Reactivity and thermal experiments

The reactivity experiments were performed in a tubular glass reactor with internal diameter of 10 mm, heated with vertical furnace with configurable temperature program. The catalyst powder was suspended on a porous glass frit and the reaction gas mixture was passed through the catalytic bed. A K-type thermocouple was inserted in the catalytic bed for continuous temperature measurement. The desired gas mixture and concentrations were adjusted through dedicated mass-flow controllers. The outlet gas composition was analyzed with ABB AO 2020 analyzers with ND-IR for NH_3 and N_2O and ND-UV for NO and NO_2 measurements and cross sensitivity of different gas species were corrected through instrument calibration. The following experiments were performed:

SCR of NO_x: 150 mg catalyst and gas flowrate of 450 mL/min with the composition of 500 ppm NO, 500 ppm NH_3, 7% O_2, 2% H_2O in N_2.

NH_3-TPD: 100 mg catalyst pretreated at 250 °C for 0.5 h in N_2 flow, followed by cooling down to 100 °C and saturation in 2000 ppm NH_3 flow. NH_3 desorption was performed in 400 mL/min N_2 flow with 5 °C/min heating rate.

NO_2-TPD: 100 mg catalyst pretreated at 250 °C for 0.5 h in N_2 flow, followed by cooling down to 100 °C and saturation in 2500 ppm NO_2 flow. NO_x desorption was performed in 400 mL/min N_2 flow with 5 °C/min heating rate. The temperature of 250 °C was chosen as it was the temperature at which the physiosorbed H_2O could be desorbed avoiding the reduction of the Fe-sites due to dehydration.

CO temperature programmed reduction (TPR): 100 mg catalyst was reduced in a flow 2000 ppm CO in He with flowrate of 250 mL/min and heating rate 5 °C/min until 650 °C. Following the reduction with CO, the catalyst was treated with 1% N_2O in He flow for 1 h at 650 °C and cooled down first to 400 °C in a N_2O flow followed by switching to a N_2 flow below 400 °C. This procedure was adopted to avoid the formation and accumulation of nitrates on the catalyst surface that would have hampered the interpretation of TPR results. The N_2O activated catalyst was reduced again in CO according to the procedure in the first step. Such procedure allowed to differentiate between the naked Fe cations and oxygen containing species in the Fe SSIE(0.25).

The H_2-TPR experiments were performed on TPDRO 1100 instrument. Typically, 60 mg of the catalyst was placed in the reactor, pretreated in He stream to remove impurities at 250 °C. Following the pretreatment, the reactor was cooled down to 50 °C and reduced in 5% H_2/Ar 20 mL/min flow, with 10 °C/min heating rate until 800 °C. The outlet gas was passed through humidity trap and analyzed with TCD detector that was previously calibrated with a CuO standard.

2.3. Characterization methods

X-ray diffraction (XRD) was performed on X′pert PW 3040 instrument with Cu anode for Kα radiation generation at 40 kV and 40 mA and passed through divergence slit. The measurements were collected in the 10–80° 2θ range with pixel array detector for continuous data acquisition.

Fourier transform infrared (FT-IR) spectroscopy was performed on Bruker Invenio S instrument with cryogenic MCT detector. The analyzed samples were pressed into thin self-supporting wafers and placed in isolated quartz glass cell with KBr windows through which the incident beam passed. Following heat treatment at relevant temperatures (r.t., 100, 250, 400 °C) for 0.5 h and evacuation at > 1 Pa the FTIR spectra were collected in transmission mode in the 4000–600 cm^{-1} range with 2 cm^{-1} resolution.

The Fe species exchanged with the SSIE procedure were probed through FT-IR measurements of low temperature CO adsorption according to the procedure described and validated in detail, in a series of spectroscopic investigations [20,28,29]. The Fe SSIE(0.25) sample was introduced in a special FT-IR cell suitable for low temperature measurements and evacuated at 400 °C for 1 h to remove any adsorbed water or impurity and cooled down with liquid N_2 to −196 °C. The CO was dosed stepwise at the controlled pressures up to 3000 Pa with spectra taken at each dosing step. Following saturation, the cell was evacuated stepwise until 2 Pa, with spectra taken at each evacuation step. The same CO-probe procedure was performed on a "reduced" Fe SSIE(0.25) sample whereby during the pretreatment step at 400 °C and 5 kPa of CO was dosed for 0.5 h, followed by evacuation for 0.5 h. The spectra reported in the Figures are differential spectra with outgassed sample as a baseline case.

Diffuse reflectance UV-Vis (DR UV-Vis) spectra of the powder samples were taken on a Cary 5000 instrument equipped with a DR sphere.

3. Results and discussion

3.1. Physico-chemical characterization

The XR diffractograms of the Fe SSIE exchanged zeolites did not show any difference from the parent SSZ-13 zeolite and the patterns relative to Fe oxides or other compounds were absent. The XR diffractogram following the ball milling contained the characteristic diffraction patterns of the parent SSZ-13 zeolite, and of $FeCl_2{\cdot}4\ H_2O$ and NH_4Cl salts (Fig. 1). The appearance of the crystalline NH_4Cl phase suggests that a proportion of the Fe cations was exchanged in the extra-framework position of the zeolite merely upon grinding at room temperature, according to the generalized reaction R1 (discussed later). The partial SSIE following the grinding could also be directly observed in the change of color: the ball milled mixture was pale orange, like the color of the final product, in contrast to the initial stark green color of $FeCl_2{\cdot}4\ H_2O$.

Following heating in He at 550 °C, $FeCl_2{\cdot}4\ H_2O$ was not detected anymore, evidencing ion exchange of the Fe in the zeolite. At temperatures around 330 °C, an increase of white deposits was observed on the wall of the outlet section of the reactor tube, where the gas exits the heated zone (Fig. S1). These white powder deposits were identified as NH_4Cl salt that was formed during the SSIE process, decomposed upon heating, and condensed when entering the cooled zone. Washing with water was not carried out at any stage of the synthesis since (the unwanted reaction product) NH_4Cl was removed by thermal decomposition, a method that would be advantageous in scaling-up the SSIE reaction to industrial scale as no wastewater would be generated.

$$NH_4\text{-SSZ-13} + FeCl_2 \rightarrow 2\ NH_4Cl + Fe^{2+}\text{-}2\ \text{SSZ-13} \quad \text{(R1)}$$

Fe-exchanged zeolites are generally characterized by high heterogeneity of the Fe species, that depends on the synthesis conditions and the zeolite properties such as the zeolite cage size and Al distribution in the zeolite framework. UV-Vis spectroscopy can provide fingerprint of the ligand-to-metal charge transfer (CT) from which some of the Fe types can be deduced, whereas the d-d electron transitions of octahedral Fe^{3+} ions (d^5 external electron configuration), being Laporte and spin forbidden, are very weak. Bands below 300 nm are generally attributed to isolated Fe^{3+} ions in the zeolite framework: more specifically, CT bands at 215 nm and 240 nm are attributed to tetrahedrally coordinated Fe^{3+} species. The band at 280 nm can be attributed to octahedrally coordinated Fe^{3+} species, dimeric -Fe-O-Fe- species or Fe^{3+} with higher number of ligands. The signal between 300 and 400 nm originates from Fe^{3+} in oligomeric Fe_xO_y clusters, whereas Fe_2O_3 particles absorb above 400 nm. It should be noted, however, that the distinction is not so clear since all the observed species have bands with Gaussian shape and a significant overlap [19,25,30–32].

The DR-UV-Vis spectra of all the Fe-SSZ-13 samples (Fig. 2) synthesized by the SSIE method showed a strong absorption below 300 nm, with an intensity increasing at higher Fe content, which means that Fe was effectively exchanged, mainly in the form of extra-framework isolated Fe^{3+} ions and iron-dimers. Except for the Fe/Al = 0.25 sample, the other SSIE prepared zeolites did not absorb significantly above 400 nm, meaning that there was no undesired formation of Fe_2O_3 particles. With the sample prepared by impregnation, a strong absorption above 400 nm indicates the undesired formation of Fe_2O_3 particles, which have detrimental effect on the catalytic activity for NO_x reduction (see Fig. 5).

Highly siliceous zeolites are difficult to investigate by classical techniques (e.g. XRD or XPS) due to low metal cation content and low symmetry of the framework structure. The IR spectroscopy technique has been suggested in a number of publications (see e.g. [15,25,32–43]) for the evidencing of ion-exchanged cationic species and consists in the observation of the signal appearing upon ion exchange in the transmission window around 900 – 950 cm^{-1}. The signal derives from the antisymmetric T-O-T vibration of the oxygen ring in TO_4 tetrahedra (T = Al, Si), which is perturbed upon the interaction with the exchanged extra-framework cation. The unperturbed T-O-T oxygen vibration is

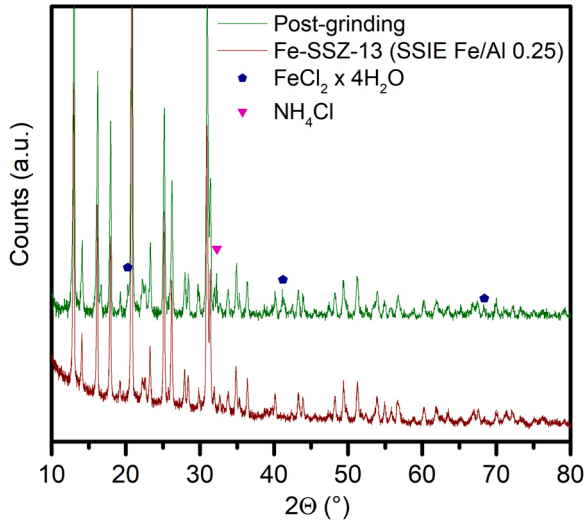

Fig. 1. XR diffractogram of the Fe SSIE(0.25) and the physical mixture of NH_4-SSZ-13 + $FeCl_2{\cdot}4\ H_2O$ after ball milling.

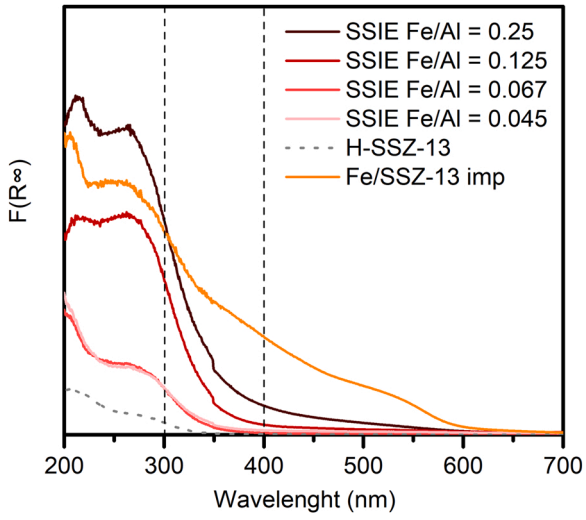

Fig. 2. DR UV–vis spectra of Fe-SSZ-13 samples synthesized by SSIE method and impregnation method.

typically located around 1100–1020 cm^{-1} that, depending on the strength of the electron interaction with the counter cation, is shifted to lower wavenumbers. Figs. 3 and 4B show this phenomenon in the SSIE zeolites, where upon the ion-exchange of Fe a band at 905 cm^{-1} appears, its intensity being roughly proportional to the exchanged Fe content. The Fe-SSIE(0.25) He (not calcined in air, but only ion exchanged in He flow) had an asymmetric perturbed signal, likely derived from the heterogeneous distribution of Fe and the probable presence of the cationic Fe^{2+} species in the zeolite.

The IR spectral region of the zeolite framework overtone vibrations (ν (T-O-T)) (Fig. S2) gives rise to four weak signals at 2000, 1870, 1690 and 1545 cm^{-1}, overlapping the band of molecular water at 1620 cm^{-1} due to water molecules either physisorbed in the zeolite channels or coordinated by Fe sites. As expected, upon evacuation above 100 °C the band at 1620 cm^{-1} disappeared, which is a strong indication that the molecular water has been completely removed. On the other hand, the hydroxyl groups (3611 and 3584 cm^{-1} bands are - related to the ν(OH) of non H-bonded bridged hydroxyls groups with a strong Brønsted acidity) remain unchanged only after treatment above 400 °C (Fig. S3) [44].

The CO probe molecule can be weakly coordinated by Fe^{2+} sites, hence its adsorption was followed by IR spectroscopy at cryogenic temperature (nominal 77 K) [20,28,29]. During CO adsorption (Fig. S4), the band at 2198 cm^{-1} is saturated first, until a CO pressure of 5 Pa is reached. This is followed by the appearance of a weak peak at 2180 cm^{-1}: as will be discussed later, such IR peaks derive from the coordination of CO molecules by Fe_xO_y oligomers. With the further increase in the partial pressure of CO, the two peaks intensity remains constant, however two broad IR signals appear at 2168 and 2140 cm^{-1}. The latter, easily removed by evacuation (Fig. 4A), is readily assigned to CO physisorption within the zeolite pores. The intensity of the 2168 cm^{-1} band, instead, grows and decreases in concert with the red shift of the hydroxyl bands in the region 3700–3300 cm^{-1}(Fig. S5), and hence is reliably assigned to CO molecules in interaction with acidic OH groups.

The CO as an IR probe molecule for Fe species has been investigated and validated by Mihaylov and Ivanova et. al in a series of detailed publications for ZSM-5 and BEA [28,29], while for SSZ-13 only one publication was found [20]. Based on these reports, the measured bands were correlated with Fe speciation and the results are shown in Fig. 4. The band at 2198 cm^{-1} was most resistant to evacuation, indicating a strong CO-site interaction, and can be assigned to Fe^{2+} species located in the 6 MR position of SSZ-13, whereas the IR signal usually corresponding to CO on Fe^{2+} species in 8 MR position at 2208 cm^{-1} was absent [20]. The likely reason is that the in 8 MR, Fe^{3+} is rather stable [20] and does not undergo reduction during the thermo-vacuum pretreatment, remaining as Fe^{3+} species, which is known as being unable to interact with CO molecules [20,28,29]. The small peak at 2180 cm^{-1} is tentatively assigned to the interaction of CO with Fe_xO_y clusters. No IR signals associated with the interaction of CO with extra-framework Al^{3+} species (at 2220–2230 cm^{-1}) were observed, suggesting that no dealumination took place during the synthesis procedure.

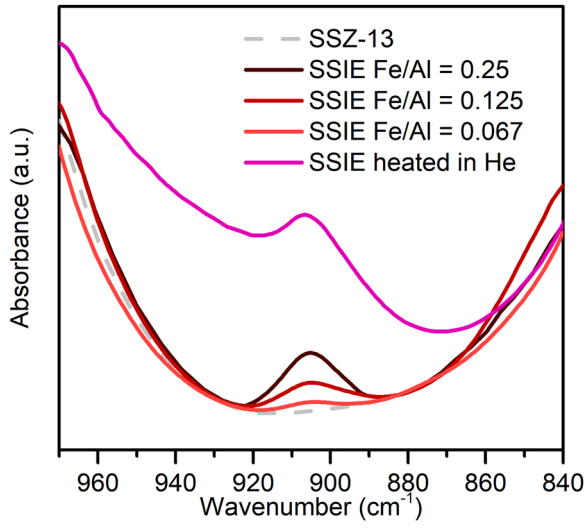

Fig. 3. FT-IR spectra of the Fe-SSZ-13 synthesized by the SSIE method in the T-O-T region evacuated at 400 °C.

The Fe^{2+} species in BEA as well as in ZSM-5 can coordinate several CO molecules, forming tri- or tetra-carbonyl complexes [29], while our observations suggest that in the case of Fe-SSZ-13 only monocarbonly species formed, in agreement with the findings in ref. [20]. This is likely the result of spatial or steric hindrance due to the confined space in the SSZ-13 zeolite cage.

The band at 905 cm^{-1}, established in the previous section to originate from T-O-T oxygen bridges perturbed by Fe cations, also underwent a significant shift (Fig. 4B) to higher wavenumbers (920 cm^{-1}) upon Fe^{2+} interaction with CO. The observed changes of the IR signal in the T-O-T region (900–950 cm^{-1}) were directly correlated solely with the band at 2198 cm^{-1}, while the interaction of CO with other components (i.e. bands at 2168 and 2140 cm^{-1}) had no such influence. This also provided an independent confirmation that the band at 2198 cm^{-1} originates from extra-framework Fe^{2+} species [20,41,43].

The FT-IR spectra on a sample previously reduced with CO at 400 °C were not different from the Fe SSIE(0.25) activated only by evacuation (Fig. S7). The absence of changes was interpreted as the trivalent Fe^{3+} species were extra-framework naked ions or, if occurring in oxygen containing species, not readily reducible. This is an important aspect, as the SCR reaction involves the redox cycling of Fe^{2+} - Fe^{3+}, hence the inert Fe^{3+} species likely do not participate in the low temperature NO_x reduction.

3.2. Catalytic activity and thermal methods of analysis

The NO_x SCR activity depends on the type of the zeolite, the framework and pore organization and Si/Al ratio. By employing Fe as active component in the NO_x SCR reaction, the larger pore zeolites, mainly BEA and ZSM-5, have been found to be more active, while small pores (e.g. SSZ-13 and SAPO-34) are slightly less efficient. The exact mechanism of the Fe-zeolite catalyzed SCR reaction is still disputed; however, the most convincing evidence suggests that the most active reaction centers are formed by dimeric Fe-O-Fe sites [21,45,46]. However, from the point of view of hydrothermal stability, small pore zeolites are significantly more resistant to hydrothermal ageing. This contrasts with the Cu-based zeolites where the small pores offer better SCR activity due to the enhanced Cu mobility in the zeolite cage and the confinement effect which prevents the N_2O formation.

Fig. 5 shows the catalytic activity for the NH_3-mediated NO_x SCR of the investigated samples. At low temperature, the samples were not active for the SCR reaction, however above 300 °C a high NO_x conversion was achieved for the Fe SSIE(0.25) and Fe SSIE(0.125) samples, comparable to the Fe-BEA. The Fe SSIE(0.067) and SSIE(0.045) samples with low Fe loading showed lower NO_x conversion likely due to the low amount of available active sites required for the reaction, therefore the increase of Fe loading proportionally increased the NO_x conversion. The Fe-SSZ-13 prepared via impregnation had a decreasing NO_x conversion above 300 °C due to the negative effect of the presence of Fe_2O_3. The SCR reaction (R4) uses NH_3 as a reductant, however concurrently the NH_3 also participates in an undesired oxidation reaction with O_2 (R5) and the ratio of the two competing reaction rates determine the efficiency of the reductant utilization. In the case of the impregnated Fe-SSZ-13 large Fe_2O_3 particles formed, that were less active for the SCR reaction and favored the NH_3 oxidation. As a consequence of the concurrent reactions R2 and R3, the NO_x conversion declined above 300 °C highlighting the importance of choosing a correct synthesis method that

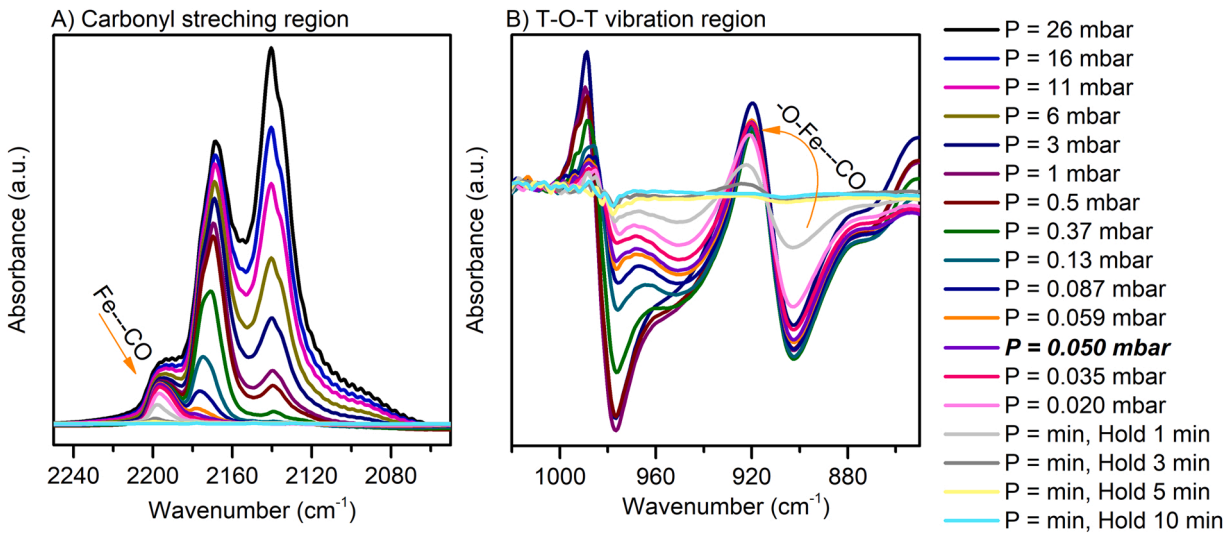

Fig. 4. Difference FT-IR spectra during the evacuation of Fe SSIE(0.25) previously saturated with CO at − 196 °C. The section A) shows the carbonyl stretching region, while section B) the T-O-T region. The adsorption stage and the corresponding hydroxyl stretching can be found in the supplementary material (Figs. S4–6).

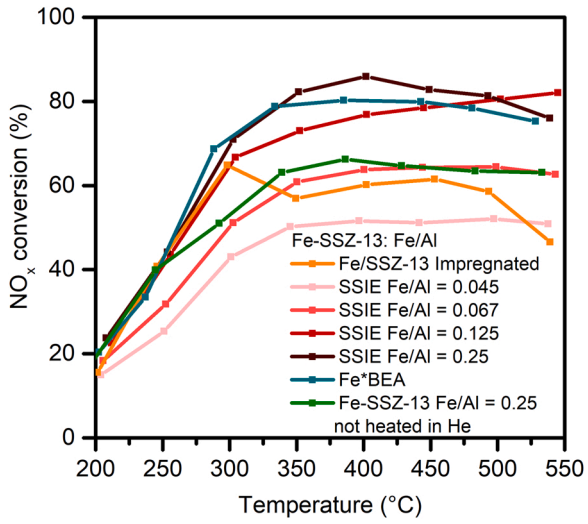

Fig. 5. The NH_3 mediated NO_x conversion over the investigated catalysts.

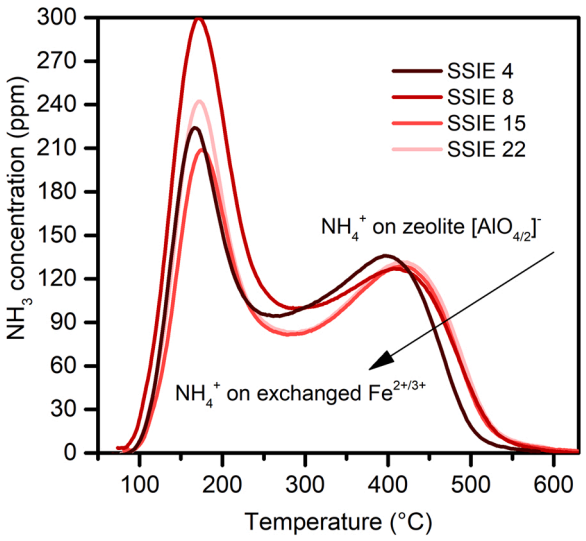

Fig. 6. Effect of Fe SSIE in the zeolite on the NH_3 adsorption capacity and acidity. The arrow indicates decreasing strength of the acid sites.

results in active ion-exchanged species. As shown by the DR UV-Vis spectra, some Fe_2O_3 particles were present in the Fe SSIE(0.25) catalyst. However, the largest amount of Fe was exchanged in extra-framework sites, which predominantly favored the NO_x SCR reaction relative to NH_3 oxidation with O_2 and there was no significant decrease in NO_x conversion at high temperature, confirming that additional Fe_2O_3 only marginally contributed to the SCR reaction. The production of undesired N_2O, was negligible for all the samples, meaning high selectivity towards N_2.

$$4\ NO + 4\ NH_3 + O_2 \rightarrow 4\ N_2 + 6H_2O \quad \text{(R2)}$$

$$4\ NH_3 + 3\ O_2 \rightarrow 2\ N_2 + 6\ H_2O \quad \text{(R3)}$$

When the catalyst was synthesised in the absence of heating under inert He flow, and calcined directly in air, had low NO_x conversion, likely due to the inhibition of the SSIE process and the ion exchange of Fe by the formation of stable FeOCl [47]. The final color of the catalyst heated only in air was dark red-violet in contrast to the orange color of the He heated SSIE prepared catalysts.

Fig. 6 shows the NH_3-TPD of the SSIE synthesized Fe-SSZ-13 with different Fe loading. The TPD can be generally differentiated in three regions depending on the desorption temperature, which can be related to the strength of the NH_3 bonding. At temperatures below 200 °C (peak at 170 °C), the desorption of physisorbed NH_3 bound by dispersive interactions and hydrogen bridging through $[NH_4^+ \cdot (NH_3)_n]$ complexes [48–50] occurs. This peak is absent in the case when water vapor is included during TPD protocol which means that weakly interacting NH_3 does not participate in the SCR reaction.

In the temperature range of 200–450 °C, the NH_3 desorbed comes from the Brønsted-type acid sites that are associated with the bridging hydroxyl groups of the zeolite, and the desorption region over 450 °C identifies the NH_3 adsorbed on the Lewis sites. According to Leistner et al. [49], H-SSZ-13 gives rise to two desorption peaks at ca. 190 °C and 510 °C, the former due to physisorbed NH_3, the latter to a combination of adsorbed ammonia mainly on Brønsted, but also Lewis, sites. Upon increasing the Fe content in the SSIE catalysts, the position of the peak of physisorbed ammonia does not change noticeably, whereas the second peak is observed at lower temperatures, indicating a consistent decrease in the binding strength of the Brønsted sites, although a contribution of NH_3 adsorbed on Lewis sites cannot be excluded, as proved by the

presence of uncoordinated Fe sites by means of infrared spectroscopy (Fig. 4). As compared to the other studied catalysts, the one with Fe/Al= 0.25 showed a more pronounced decrease of the strength of the Brønsted sites, however the total amount of chemisorbed NH_3 remained constant (516 μmol NH_3/g_{cat}), irrespective of the amount of exchanged Fe. According to the literature, the availability of NH_4^+ species strongly affects the performance of the catalyst in the SCR reaction, increasing the NO_x conversion by decreasing the strength of the Brønsted sites [51, 52].

The use of NO_2 adsorption-desorption as probe reaction for the identification of active sites participating in the SCR reaction has been validated extensively, the most detailed being by Iwasaki et al. for Fe-exchanged ZSM-5 [32,41] and the research group at Politecnico di Milano for both Cu- and Fe-zeolites [53,54]. Based on the reactivity studies and instrumental analysis, Iwasaki et al. suggested a reaction mechanism according to R6, that involves a dimeric (or multinuclear) Fe site with hexagonal coordination whereby the NO_2 adsorbs in the shared oxygen vacancy. The NO evolution during the adsorption can be explained by the NO_2 decomposition when filling up the vacancy and disproportionation according to the reaction R4. On the other hand, other publications [53,54] questioned this vacancy theory of Iwasaki and instead proposed a single Fe site mechanism (R5 and R6), similar to the mechanisms proposed for the NO_2 adsorption on Ba-based NO_x traps [55]. We see no reason why these two theories should be mutually exclusive, and, considering that the Fe distribution in zeolites is heterogeneous and highly dependent on the synthesis conditions, they can rather be seen as complementary. In this manner, the variability of the reported ratio between the adsorbed NO_2 and the simultaneous evolution of NO [53,54] can be explained in a straightforward manner, as well as the appearance of multiple desorption peaks.

$$Z\text{-}[(HO)Fe\text{-}O\text{-}Fe(OH)]^{2+} \text{-}Z + 6\ NO_2 \rightarrow 2Z\text{-}Fe(NO_3)_2 + H_2O + 2\ NO \quad (R4)$$

$$Z\text{-}Fe^{3+}\ (OH)\ \text{-}Z + 3\ NO_2 \rightarrow Z^+ + Z\text{-}Fe^{3+}(NO_3)_2 + NO \quad (R5)$$

$$Z\text{-}Fe^{3+}\ (OH)_2 + 3\ NO_2 \rightarrow Z\text{-}Fe^{3+}(NO_3)_2 + NO + H_2O \quad (R6)$$

The BEA zeolite framework is favorable towards the formation of dimeric Fe species when the synthesis is performed in well controlled conditions, and as shown in Fig. 7 a single large peak between 250 and 350 °C, as well as a large amount of NO released during the adsorption phase, evidence the preferential formation of such extra-framework Fe species. The SSIE synthesized Fe-SSZ-13 showed a more complex desorption profile. At low Fe loading the peak at high temperature was dominant, suggesting that in the initial stages of the SSIE reaction the Fe is exchanged preferentially as dimers. The sites that can accommodate dimeric Fe species seem to be limited, likely with the availability of at least two $[AlO_{4/2}]^-$ sites in the zeolite 6 MR and 8 MR rings and their distribution in the zeolite cage. Following the saturation by the dimeric species, the Fe is exchanged as isolated Fe^{3+}, characterized with the NO_2 desorption peak at 150 °C, and confirmed with spectroscopic techniques. Based on the NO_2 desorption, the proportion of the $[AlO_{4/2}]^-$ sites during the SSIE process that are able to form a dimeric Fe species is estimated to be 10–15%, while the rest can form only isolated Fe species [56,57]. This high exchange site diversity observed for the SSZ-13, in contrast with the BEA type framework, is likely the consequence of the different structure of the zeolites, size of the channels and cages and Al distribution. In particular, the Al distribution has been thought to be largely random in zeolites, with some limitation such as the Löwenstein rule that forbids Al-O-Al pairings [56,57].

The H_2-TPR curves of the investigated samples are shown in the Fig. 8. The Fe-BEA reduction presented a single peak, that was likely related to the dimeric Fe cations that preferentially form in this zeolite framework and corresponded well with the results obtained from the NO_2-TPD. The Fe-SSZ-13 catalysts showed a more heterogenous distribution that was not possible to deconvolute and interpret unambiguously. The heterogeneity of Fe species is consistent with the results from the previous experiments and instrumental analyses and it is likely the result of the presence of dimeric Fe species, isolated Fe cations, Fe-oxo species and possibly oxide like Fe_xO_y oligomers.

H_2 can reduce all the Fe types, however CO can access and react only with O-containing Fe species. Hence CO-TPR was used to differentiate between oxocations and Fe ions. Indeed, the CO did not react with the Fe SSIE(0.25) until above 400 °C that proved that the oxide like Fe_2O_3 is largely absent and the oxygen content of the sample is low (Fig. S7). Reaction of Fe zeolites with N_2O can generate α-oxygen that is highly reactive and cannot be obtained from molecular O_2 as oxidant. The CO-TPR of the Fe- SSIE(0.25) was markedly different following N_2O treatment with the presence of a number of highly reactive oxygen, not found in the air activated Fe SSIE(0.25).

The numerical result of the characterization is presented in Table 1. The relative reducibility of the Fe species decreases with increasing the Fe content. This occurrence was supported by the other characterization techniques as it was demonstrated that increasing the extent of ion exchange the ratio of the stable isolated Fe^{3+} species and Fe_xO_y oligomers increased that were less reducible in the investigated temperature range.

The total pore volume was not correlated with the total Fe content exchanged during the SSIE that indicated uniform distribution of the exchanged Fe and that any Fe_2O_3 or Fe_xO_y particles that might have formed did not block the zeolite channels or cages. The minor reduction

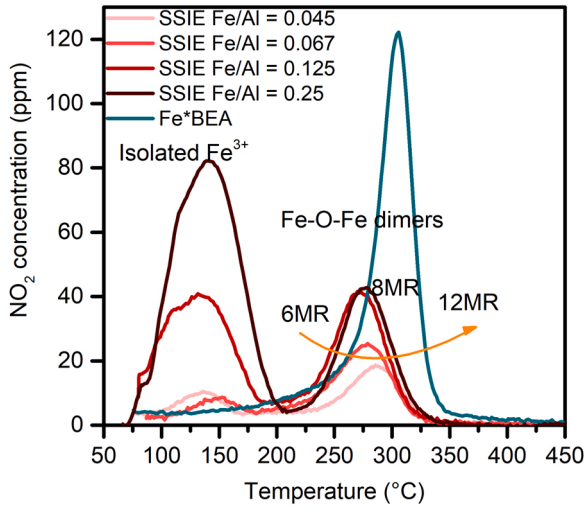

Fig. 7. NO_2-TPD over the Fe-SSZ-13 SSIE synthesized catalysts.

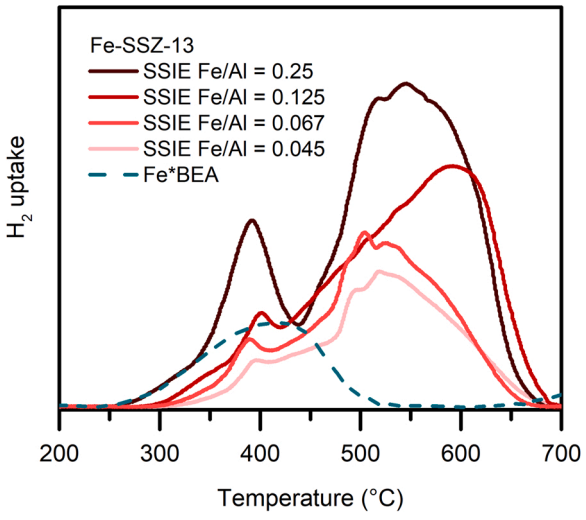

Fig. 8. The H_2-TPR of the Fe SSIE samples.

in volume relative to the starting H-SSZ-13 zeolite is likely the result of the heat treatment during synthesis.

4. Discussion

During the SSIE process the Fe cations were introduced in highly dispersed extra-framework zeolite position. The UV–vis spectroscopy provided a fingerprint of the Fe heterogeneity in the zeolite, other complementary characterization identified the variety of the Fe species. It is plausible that the stable Fe^{3+} species form- in the zeolite included as naked cations as well as species with formal charge per Fe lower than 3, i.e. hydroxy-cations $[Fe(OH)_2]^+$ (or $[Fe(OH)]^{2+}$) as well as dimeric cations connected via an oxygen bridge $[(HO)Fe\text{-}O\text{-}Fe(OH)]^{2+}$. The SSZ-13 cage structure consists of interconnected tetrahedra (T-O-T) that form 6 MR and 8 MR rings on which the Fe cations can be exchanged. The Si/Al ratio in the investigated zeolites was 9 and, as a general rule, the $[AlO_{4/2}]^-$ exchange sites are stochastically distributed through the zeolite framework and the 6 MR and 8 MR rings can contain one, two or no $[AlO_{4/2}]^-$ site. From a statistical perspective the proportion of the dimeric species should decrease with the increase in the Fe species, assuming stochastic Fe distribution. This was demonstrated to be only partially true since the exchange process proceeded in an ordered manner with the Fe exchanging preferentially as dimers on sites where two $[AlO_{4/2}]^-$ next nearest neighbor are available and only after saturating these sites Fe is exchanged on isolated $[AlO_{4/2}]^-$ sites. This phenomenon has been decidedly demonstrated for the Cu-exchanged SSZ-13 [44,58,59]. The BEA zeolite consists of 12 MR where the population of the two $[AlO_{4/2}]^-$ sites are statistically much more probable and can accommodate higher number of dimeric Fe.

The low energy ball-milling resulted in a physical powder mixture of the NH_4-SSZ-13 and $FeCl_2{\cdot}4\ H_2O$ in what is commonly called as “tight contact”. This involved the dispersion of the $FeCl_2{\cdot}4\ H_2O$ salt particles, with diameter between 1 and 100 μm, on the zeolite particle surface, without the salt entering the pores. Based on previous publications (see e.g. [10,11,18,26,33]), the water molecules in the hydrated salt were considered to have no influence on the SSIE reaction or participate in the ion-exchange process. The question arises, what is the driving force of the solid-state exchange and the manner in which the ions migrate on micrometric length scale, in the absence of solvated intermediate. The $[AlO_{4/2}]^-$ sites can act as powerful ion traps e.g. the CuO or Cr_3O_4 can be SSIE in the H-form of the zeolite merely upon heating [10,12,58,60]. This is not the case for Fe since the mixture of Fe_2O_3 and H-zeolite does not react. The SSIE exchange of Fe can take place only if a stable ionic salt of Fe is applied, which does not produce oxide like decomposition product, the NH_4-form of the zeolite is used and only if heated in O_2-free atmosphere. A plausible explanation could be that the SSIE of Fe is analogous to the double displacement reaction with the ions “flowing” through the zeolite-salt interface and exchanging the two NH_4^+ cations with the Fe^{2+}. This proposed SSIE mechanism has however several issues. The concerted motion of multiple ions would have to be strictly correlated and during the process lattice distortion, with the consequent higher energy barrier, would be expected in both the zeolite and $FeCl_2$. An alternative explanation could be a stepwise mechanism whereby the Cl^- and NH_4^+ ions react first and the $FeCl^+$ is trapped by the liberated vacancy:

$$Z\text{-}NH_4 + FeCl_2 \rightarrow Z\text{-}FeCl^+ + NH_4Cl \quad (R7)$$

The $[FeCl^+]$ complex is not stable and the chloride further reacts with NH_4^+ in the zeolite:

$$Z\text{-}NH_4 + Z\text{-}FeCl^+ \rightarrow 2\ Z\text{-}Fe^{2+} + NH_4Cl \quad (R8)$$

The exchanged Fe ions can recombine to form dimers when suitable environment, i.e. $[AlO_{4/2}]^-$ pairs in a ring, is present.

$$Z\text{-}(NH_4)_2^{2+} + Fe_2Cl_4 \rightarrow 2\ Z\text{-}[Fe\text{-}\square\text{-}Fe]Cl_2 + 2\ NH_4Cl \quad (R9)$$

It should be noted that in the above scheme multiple types of “Z” sites can be present depending on the location (6 MR or 8 MR) in the zeolite and the number of available $[AlO_{4/2}]^-$ sites. From the reactions, it is evident that the maximum Fe/Al ratio achievable with SSIE method is 0.5.

In the reaction system above, the NH_4Cl salt that formed during the SSIE reaction was decomposed when the reaction temperature was above 320 °C and could be observed as white powder that spontaneously deposited when exiting from the heated zone. In the final product no chloride could be observed suggesting full conversion during the SSIE.

However, the question arises regarding the overall thermodynamic driving force of SSIE and changes in the chemical potential and Gibbs energy. In some SSIE reactions involving Cu in zeolites, the final product is the Cu-exchanged zeolite and gaseous reaction product (i.e. HCl) and in this case there is a positive contribution of the entropy increase to the thermodynamics. In our case, both the starting materials (NH_4-SSZ-13 and $FeCl_2{\cdot}4\ H_2O$) and the reaction products (Fe-SSZ-13 and NH_4Cl) are well ordered, solid state crystalline materials and the change in entropy can be presumed to be negligible. The main contribution to the change in the Gibbs free energy is thought to derive from the change in the enthalpy.

5. Conclusions

The SSIE technique can be a preferable alternative to the commonly used liquid ion exchange for the introduction of Fe cations in the small pore SSZ-13 zeolite. During the SSIE process, the $FeCl_2$ salt reacts with NH_4^+ ions at the zeolite exchange sites to form the Fe-SSZ-13 and NH_4Cl. As evidenced by spectroscopic (UV-Vis, FT-IR) and thermal desorption (NO_2 and NH_3-TPD) techniques, the exchange process is sequential as the Fe cations preferentially exchange in environments where at least two $[AlO_{4/2}]^-$ sites are available forming [Fe-O-Fe] dimers. Once these sites are occupied, isolated, single site Fe cations are formed. The migration of the ions is induced upon contact grinding at room temperature and enhanced during heating in inert He atmosphere. The thermodynamic driving force appear to be the change in the enthalpy of the reaction rather than entropic.

The SSIE reaction can be a simple and highly effective synthesis method for producing ion exchanged small pore zeolites with different extra-framework Fe species. The extent of ion exchange can be controlled to produce active sites required for specific catalytic reactions. This is an important improvement in contrast to the classical wet-ion exchange of Fe in small pore zeolites.

CRediT authorship contribution statement

Ferenc Martinovic: Conceptualization, Methodology, Investigation, Formal analysis, Writing – original draft, Writing – review & editing. **Sabrina Ballauri:** Methodology, Investigation. **Nicola Blangetti:** Methodology, Investigation. **Samir Bensaid:** Conceptualization, Writing – review & editing, Supervision. **Raffaele Pirone:** Supervision. **Barbara Bonelli:** Validation, Formal analysis, Writing – original draft, Writing – review & editing. **Marco Armandi:** Investigation, Formal analysis. **Fabio Alessandro Deorsola:** Conceptualization, Formal analysis, Writing – original draft, Writing – review & editing, Supervision.

Declaration of Competing Interest

The authors declare that they have no known competing financial interests or personal relationships that could have appeared to influence the work reported in this paper.

Data Availability

Data will be made available on request.

Appendix A. Supporting information

Supplementary data associated with this article can be found in the online version at doi:10.1016/j.apcata.2023.119160.

References

[1] T.C. Watling, M.R. Ravenscroft, G. Avery, Catal. Today (2012) 32–41.
[2] P.S. Metkar, M.P. Harold, V. Balakotaiah, Appl. Catal. B Environ. 111–112 (2012) 67–80.
[3] W. Tang, B. Chen, K. Hallstrom, A. Wille, SAE Int. J. Engines 9 (2016).
[4] F. Martinovic, L. Castoldi, F.A. Deorsola, 653 11, Catal 2021 Vol. 11 (2021) 653.
[5] D. Zhang, R.T. Yang, Energy Fuels 32 (2018) 2170–2182.
[6] J. Wang, H. Zhao, G. Haller, Y. Li, Appl. Catal. B Environ. 202 (2017) 346–354.
[7] Q. Ye, L. Wang, R.T. Yang, Appl. Catal. A Gen. 427–428 (2012) 24–34.
[8] F. Gao, C.H.F. Peden, Catalysts 8 (2018).
[9] Y. Shan, W. Shan, X. Shi, J. Du, Y. Yu, H. He, Appl. Catal. B Environ. 264 (2020), 118511.
[10] H.G. Karge, H.K. Beyer, Stud. Surf. Sci. Catal. 69 (1991) 43–64.
[11] H.G. Karge, Handb Heterog, Catal (2008) 484–510.
[12] A.V. Kucherov, A.A. Slinkin, J. Mol. Catal. 90 (1994) 323–354.
[13] A.V. Kucherov, A.A. Slinkin, Russ. Chem. Rev. 61 (1992) 925–943.
[14] A.K.S. Clemens, A. Shishkin, P.A. Carlsson, M. Skoglundh, F.J. Martínez-Casado, Z. Matej, O. Balmes, H. Härelind, A.C.S. Catal. 5 (2015) 6209–6218.
[15] R. Charrad, H.E. Solt, J. Valyon, L. Trif, F. Ayari, M. Mhamdi, J. Hancsók, F. Lónyi, ChemistryOpen 9 (2020) 1123–1134.
[16] M. Armandi, T. Andana, S. Bensaid, M. Piumetti, B. Bonelli, R. Pirone, Catal. Today 345 (2020) 59–70.
[17] C. Jia, P. Beaunier, P. Massiani, Microporous Mesoporous Mater. 24 (1998) 69–82.
[18] H.G. Karge, V. Mavrodinova, Z. Zheng, H.K. Beyer, Appl. Catal. 75 (1991) 343–357.
[19] F. Gao, Y. Zheng, R.K. Kukkadapu, Y. Wang, E.D. Walter, B. Schwenzer, J. Szanyi, C.H.F. Peden, A.C.S. Catal. 6 (2016) 2939–2954.
[20] J. Szanyi, F. Gao, J.H. Kwak, M. Kollár, Y. Wang, C.H.F. Peden, Phys. Chem. Chem. Phys. 18 (2016) 10473–10485.
[21] L. Kovarik, N.M. Washton, R. Kukkadapu, A. Devaraj, A. Wang, Y. Wang, J. Szanyi, C.H.F. Peden, F. Gao, A.C.S. Catal. 7 (2017) 2458–2470.
[22] F. Martinovic, F.A. Deorsola, M. Armandi, B. Bonelli, R. Palkovits, S. Bensaid, R. Pirone, Appl. Catal. B Environ. 282 (2021).
[23] M. Ogura, K. Itabashi, J. Dedecek, T. Onkawa, Y. Shimada, K. Kawakami, K. Onodera, S. Nakamura, T. Okubo, J. Catal. 315 (2014) 1–5.
[24] Y. Kobatake, K. Momma, S.P. Elangovan, K. Itabashi, T. Okubo, M. Ogura, ChemCatChem 8 (2016) 2516–2524.
[25] L. Čapek, V. Kreibich, J. Dědeček, T. Grygar, B. Wichterlová, Z. Sobalík, J. A. Martens, R. Brosius, V. Tokarová, Microporous Mesoporous Mater. 80 (2005) 279–289.
[26] K. Lazar, G. Pal-borbely, H.K. Beyer, J. Chem. Soc., Faraday Trans. 90 (1994) 1329–1334.
[27] M. Rauscher, K. Kesore, R. Mönnig, W. Schwieger, A. Tißler, T. Turek, Appl. Catal. A Gen. 184 (1999) 249–256.
[28] E. Ivanova, M. Mihaylov, K. Hadjiivanov, V. Blasin-Aubé, O. Marie, A. Plesniar, M. Daturi, Appl. Catal. B Environ. 93 (2010) 325–338.
[29] M. Mihaylov, E. Ivanova, K. Chakarova, P. Novachka, K. Hadjiivanov, Appl. Catal. A Gen. 391 (2011) 3–10.
[30] J.P. Pariente, M. Sánchez-Sánchez, Structure and Reactivity of Metals in Zeolite Materials, 2018.
[31] M.L. Bols, J. Devos, H.M. Rhoda, D. Plessers, E.I. Solomon, R.A. Schoonheydt, B. F. Sels, M. Dusselier, J. Am. Chem. Soc. 143 (2021) 16243–16255.
[32] M. Iwasaki, K. Yamazaki, K. Banno, H. Shinjoh, J. Catal. 260 (2008) 205–216.
[33] E. Tabor, M. Lemishka, Z. Sobalik, K. Mlekodaj, P.C. Andrikopoulos, J. Dedecek, S. Sklenak, Commun. Chem. 2 (2019) 1–9.
[34] P. Sazama, N.K. Sathu, E. Tabor, B. Wichterlová, Š. Sklenák, Z. Sobalík, J. Catal. 299 (2013) 188–203.
[35] Y. Ganjkhanlou, E. Groppo, S. Bordiga, M.A. Volkova, G. Berlier, Microporous Mesoporous Mater. 229 (2016) 76–82.
[36] P. Boroń, L. Chmielarz, J. Gurgul, K. Łatka, T. Shishido, J.M. Krafft, S. Dzwigaj, Appl. Catal. B Environ. 138–139 (2013) 434–445.
[37] M. Mauvezin, G. Delahay, B. Coq, S. Kieger, J.C. Jumas, J. Olivier-Fourcade, J. Phys. Chem. B 105 (2001) 928–935.
[38] R. Millan, P. Cnudde, A.E.J. Hoffman, C.W. Lopes, P. Concepción, V. Van Speybroeck, M. Boronat, J. Phys. Chem. Lett. 11 (2020) 10060–10066.
[39] J. Sárkány, Appl. Catal. A. Gen. 188 (1999) 369–379.
[40] E. Broclawik, J. Datka, B. Gil, P. Kozyra, Phys. Chem. Chem. Phys. 2 (2000) 401–405.
[41] M. Iwasaki, H. Shinjoh, J. Catal. 273 (2010) 29–38.
[42] J. Sárkány, Phys Chem, Chem. Phys. 1 (1999) 5251–5257.
[43] J. Sárkány, Appl Catal, A. Gen 229 (2002) 291–312.
[44] E. Borfecchia, K.A. Lomachenko, F. Giordanino, H. Falsig, P. Beato, A.V. Soldatov, S. Bordiga, C. Lamberti, Chem. Sci. 6 (2015) 548–563.
[45] K. Kamasamudram, N. Currier, T. Szailer, A. Yezerets, SAE Int. J. Fuels Lubr. 3 (2010) 664–672.
[46] F. Gao, M. Kollár, R.K. Kukkadapu, N.M. Washton, Y. Wang, J. Szanyi, C.H. F. Peden, Appl. Catal. B Environ. 164 (2015) 407–419.
[47] K. Adam, I. Iwasaki, Miner. Metall. Process. 1984 13 (1) (1984) 190–196.
[48] F. Lónyi, J. Valyon, Microporous Mesoporous Mater. 47 (2001) 293–301.
[49] K. Leistner, K. Xie, A. Kumar, K. Kamasamudram, L. Olsson, Catal. Lett. 147 (2017) 1882–1890.
[50] G. Boskovic, T. Vulic, E. Kis, P. Putanov, Chem. Eng. Technol. 24 (2001) 269–274.
[51] P. Chen, M. Jabłońska, P. Weide, T. Caumanns, T. Weirich, M. Muhler, R. Moos, R. Palkovits, U. Simon, A.C.S. Catal. 6 11 (2016) 7696–7700.
[52] A. Grossale, I. Nova, E. Tronconi, J. Catal. 265 (2009) 141–149.
[53] M.P. Ruggeri, T. Selleri, M. Colombo, I. Nova, E. Tronconi, J. Catal. 311 (2014) 266–270.
[54] M. Colombo, I. Nova, E. Tronconi, Appl. Catal. B Environ. 111–112 (2012) 433–444.
[55] P.J. Schmitz, R.J. Baird, J. Phys. Chem. B 106 (2002) 4172–4180.
[56] C. Paolucci, A.A. Parekh, I. Khurana, J.R. Di Iorio, H. Li, J.D. Albarracin Caballero, A.J. Shih, T. Anggara, W.N. Delgass, J.T. Miller, F.H. Ribeiro, R. Gounder, W. F. Schneider, J. Am. Chem. Soc. 138 (2016) 6028–6048.
[57] R.E. Fletcher, S. Ling, B. Slater, Chem. Sci. 8 (2017) 7483–7491.
[58] A.K.S. Clemens, A. Shishkin, P.A. Carlsson, M. Skoglundh, F.J. Martínez-Casado, Z. Matej, O. Balmes, H. Härelind, A.C.S. Catal. 5 (2015) 6209–6218.
[59] F. Göltl, R.E. Bulo, J. Hafner, P. Sautet, J. Phys. Chem. Lett. 4 (2013) 2244–2249.
[60] P.N.R. Vennestrøm, L.F. Lundegaard, C. Tyrsted, D.A. Bokarev, A.I. Mytareva, G. N. Baeva, A.Y. Stakheev, T.V.W. Janssens, Top. Catal. 62 (2019) 100–107.